PAPER

Optimal Design of Wideband mmWave LoS MIMO Systems Using Hybrid Arrays with Beam Squint*

Yongpeng HU[†], **Hang LI**[†a)], **J. Andrew ZHANG**[††], **Xiaojing HUANG**[††], ***and*** **Zhiqun CHENG**[†], ***Nonmembers***

SUMMARY Analog beamforming with broadband large-scale antenna arrays in millimeter wave (mmWave) multiple input multiple output (MIMO) systems faces the beam squint problem. In this paper, we first investigate the sensitivity of analog beamforming to subarray spatial separations in wideband mmWave systems using hybrid arrays, and propose optimized subarray separations. We then design improved analog beamforming after phase compensation based on Zadoff-Chu (ZC) sequence to flatten the frequency response of radio frequency (RF) equivalent channel. Considering a single-carrier frequency-domain equalization (SC-FDE) scheme at the receiver, we derive low-complexity linear zero-forcing (ZF) and minimum mean squared error (MMSE) equalizers in terms of output signal-to-noise ratio (SNR) after equalization. Simulation results show that the improved analog beamforming can effectively remove frequency-selective deep fading caused by beam squint, and achieve better bit-error-rate performance compared with the conventional analog beamforming.

key words: *mmWave, LoS MIMO, hybrid arrays, beam squint, SC-FDE*

1. Introduction

With the explosive growth in mobile data usage, pursuing higher spectral efficiency and reliability has become the main theme of future wireless communication system design [1]. Currently, the microwave resource in low frequency bands is in short supply, and cannot provide more bandwidth for high-speed communications. Therefore, more attention is turned to the millimeter wave (mmWave) with higher frequency, which is an effective way to solve the shortage of spectrum resource [2], [3]. It is proved that the existing point-to-point mmWave communication systems can achieve multigigabit data rates at a distance of up to a few kilometers [4]. However, its propagation characteristics of large path loss, significant attenuation and poor diffraction penetration limit the transmission capacity.

Thanks to the short wavelength of mmWave, more antenna elements can be deployed in the limited space. This practically allows massive multiple input multiple output (MIMO) to overcome the path loss through beamforming with high accuracy and gain [5]. Also, massive MIMO with multiple radio frequency (RF) chains enables spatial multiplexing with multistream transmission for high spectral efficiency, and adaptation of radiation patterns for beam gains via adaptive beamforming using antenna arrays [6], [7]. As a result, it is becoming increasingly attractive to consider mmWave MIMO communications as an alternative for the emerging 6G communications. The full-digital array structure is generally used in traditional low frequency MIMO systems with a small number of antennas, while analog-digital hybrid arrays are mostly adopted for mmWave massive MIMO systems [8]. Although the former is seamlessly compatible with conventional MIMO and able to achieve the optimal performance in terms of transmission rate, its implementation for large-scale antenna arrays would incur prohibitive cost. On the other hand, hybrid arrays turn out to be a cost-efficient and feasible solution [9]. It can not only effectively provide sufficient power and high directivity by adjusting the phases of signals, but also realize spatial multiplexing and multi-user MIMO using multiple RF chains [10], [11].

MmWave channels are commonly featured by sparse scattering, and thus seem to be opposed to conventional spatial multiplexing. Generally, the line-of-sight (LoS) component dominates in a typical mmWave propagation environment, leading to the MIMO channel matrix with a high possibility of insufficient rank. However, it has been proved that a high-rank channel matrix and full spatial multiplexing gain can be achieved in a pure LoS environment using an appropriately designed array [12]. Relevant works in [13]-[15] were proposed to optimize spatial multiplexing and mutual information by solving the orthogonal relationship of the channel matrix for uniform linear array (ULA), uniform circular array and uniform planar array, respectively. It is found that the optimal performance can be obtained only when the system parameters satisfy the Rayleigh distance criterion. In general, it refers to the condition that the communication distance R between the transmitter (Tx) and the receiver (Rx) should be equal to or less than the so-called Rayleigh distance, i.e., $R \leq VS_tS_r\cos\theta/\lambda$, where S_tS_r is the antenna separation product, λ is the carrier wavelength, V is the maximum number of antennas of the Tx and Rx, and θ is the angle of local spherical coordinate system at the Rx. Besides, the optimal subarray separation design for hybrid arrays was studied to meet Rayleigh distance criterion in [16]. The existing research on Rayleigh distance criterion mainly focuses on narrowband systems. For wideband systems with a relatively large bandwidth, different signal frequencies (wavelengths) will impact on the Rayleigh distance

[†]The authors are with the School of Electronics and Information, Hangzhou Dianzi University, Hangzhou 310018, China.

[††]The authors are with The Global Big Data Technologies Centre, University of Technology Sydney, Sydney 2007, Australia.

*This work is supported by National Key R&D Program of China (Grant:2018YFE0207500), National Natural Science Foundation (Grant 62071163), Zhejiang Provincial Natural Science Foundation (Grant LY22F010003) and Project of Ministry of Science and Technology (Grant D20011).

a) E-mail: hangli@hdu.edu.cn

DOI: 10.1587/transcom.E0.B.1

criterion thus the optimal design for arrays. The relevant work is few, but it is important and deserves further investigation.

With the increase of bandwidth and array size, the propagation delay across different antennas becomes non negligible, which is called spatial wideband effect and causes beam squint in frequency-domain [17]. Essentially, beam squint means that the beam direction varies with frequency, leading to the frequency dependent channel. There are some existing literature referring the beam squint issue. The true time delay (TTD) lines provide a programmable true time delay by introducing the varying phases over frequencies, and can perfectly mitigate beam squint [18]. However, due to the high implementation cost and power consumption, it's impractical to apply TTD lines to resolve beam squint in mmWave communication systems. A phased array codebook is designed to enhance the minimum array gain of all subcarriers in wideband systems [19]. In [20], an advanced analog beamforming method for phased arrays is used to eliminate frequency-selective deep fading in the RF equivalent channel. In [21], a subarray is divided into several smaller subarrays, and their phases are separately compensated to reduce the beam squint effect. An array structure with a few TTD lines is proposed to achieve near optimal performance under the premise of controllable power consumption and complexity. In [22], beam squint is alleviated by adding a well-designed spatial dimension frequency modulation waveform to the phase shifter. All the aforementioned existing works are limited to specific scenarios or with high complexity, and do not consider beam squint in mmWave LoS MIMO systems using hybrid arrays.

In order to optimize the system spectral efficiency, we investigate the effect of frequency-dependency on subarray separation design based on Rayleigh distance criterion in wideband mmWave LoS MIMO systems using hybrid arrays in this paper. It is shown that the subarray separations designed under the carrier frequency can achieve the maximum spectral effciency. With the optimal subarray separations, we then analyze the influence of beam squint on RF equivalent channel, which illustrates that beam squint can cause frequency-selective deep fading and thus serious loss with the increasing bandwidth and array size. To reduce the adverse impact of beam squint, we design the phase shifter values for the improved analog beamforming by multiplying a Zadoff-Chu (ZC) sequence to the phase shifters of the conventional beamforming for each subarray, which can availably smooth the frequency-domain response of the RF equivalent channel. With the improved analog beamforming, we analyze the equalization performance in term of output signal-to-noise ratio (SNR) after equalization using zero-forcing (ZF) and minimum mean squared error (MMSE) based equalizers in a single-carrier frequency-domain equalization (SC-FDE) system. Simulation results show that the improved analog beamforming can effectively mitigate frequency-selective deep fading and inter-symbol interference (ISI) for wideband mmWave LoS MIMO systems using hybrid arrays integrated with the SC-FDE scheme, achieving superior bit-error-rate (BER) performance to conventional beamforming.

The rest of this paper is organized as follows. Section 2 introduces the signal and channel models. In section 3, we explore the optimal design of subarray separations in wideband systems. Section 4 analyzes the beam squint effect and presents the improved analog beamforming for removing the frequency-selective deep fading. In section 5, we present SC-FDE using the improved analog beamforming in wideband mmWave LoS MIMO systems. Its effectiveness is demonstrated by simulation results in Section 6. Finally, Section 7 concludes this paper.

The following notions are used throughout this paper. $\mathbf{A}^T$ and $\mathbf{A}^H$ denote the transpose and the conjugate transpose of matrix $\mathbf{A}$, respectively; $\mathcal{CN}(0, \mathbf{A})$ represents the zero-mean complex Gaussian distribution with covariance matrix $\mathbf{A}$; $|\cdot|$ denotes the determinant operation; $\|\cdot\|$ denotes Frobenius norm of matrix $\mathbf{A}$; $diag(\mathbf{a})$ is a matrix whose diagonal elements are formed by $\mathbf{a}$; $E\{\cdot\}$ is the expectation operator; $\mathbf{I}$ is the identity matrix; and $\odot$ denotes the Hadamard product.

2. System Model

2.1 Signal Model

A single user wideband mmWave MIMO downlink system using hybrid array is considered in this paper. As shown in Fig. 1, the Tx and Rx with partially connected ULA are equipped with N and M subarrays, respectively. Each Tx or Rx subarray has P or Q antenna elements, respectively, and is connected with one RF chain with multiple phase shifters which are used to implement analog beamforming. Due to the limitations of hardware conditions and signal processing capabilities, users side as a Rx usually has fewer antennas. Assume a bandwidth of B and denote the discrete frequency-domain channel response matrix as $\mathbf{H}[k] \in \mathbb{C}^{MQ\times NP}$, where the index k represents a discrete frequency $f_k = \frac{kB}{K} - \frac{B}{2}$, $k = 0, 1, ..., K-1$, and K represents the total number of discrete frequencies. Without loss of generality, assuming that the number of data stream N_s is equal to N, the complex output signal $\mathbf{y}[k] = [y_0[k], y_1[k], ..., y_{M-1}[k]]^T$ after analog combining can be represented as

$$\mathbf{y}[k] = \mathbf{W}^H\mathbf{H}[k]\mathbf{F}\mathbf{x}[k] + \mathbf{W}^H\mathbf{n}[k] = \widetilde{\mathbf{H}}[k]\mathbf{x}[k] + \overline{\mathbf{n}}[k], \quad (1)$$

where $\mathbf{x}[k] \in \mathbb{C}^{N\times 1}$ and $\mathbf{n}[k] \in \mathbb{C}^{MQ\times 1}$ denote the frequency-domain transmitted signal vector and the additional white Gaussian noise vector with distribution $\mathcal{CN}(0, \sigma^2\mathbf{I}_{MQ})$, respectively, and σ^2 is the noise power. $\widetilde{\mathbf{H}}[k] = \mathbf{W}^H\mathbf{H}[k]\mathbf{F}$ denotes the RF equivalent channel, $\mathbf{F} \in \mathbb{C}^{NP\times N}$ and $\mathbf{W} \in \mathbb{C}^{MQ\times M}$ denote the analog precoding matrix and analog combining matrix at the Tx and Rx, respectively. Specifically, $\mathbf{F}$ and $\mathbf{W}$ can be expressed as

$$\mathbf{F} = diag(\mathbf{f}_0, \mathbf{f}_1, ..., \mathbf{f}_{N-1}) \quad (2)$$

and

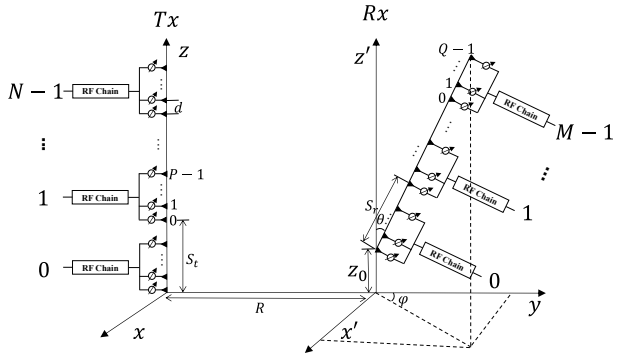

Fig. 1 Antennas layout for subarray structure.

$$\mathbf{W} = diag(\mathbf{w}_0, \mathbf{w}_1, ..., \mathbf{w}_{M-1}), \tag{3}$$

respectively, where $\mathbf{f}_n$ and $\mathbf{w}_m$ are the normalized array factors of the nth and mth array factors of the transmit and receive subarrays respectively.

Assuming that the channel state information is perfectly known at the Rx and equal power transmission for each subchannel is used, the spectral efficiency of the above described wideband system is given by [23]

$$SE = \frac{1}{K}\sum_{k=0}^{K-1}\log_2\left(\left|\mathbf{I}_N + \frac{\gamma}{U}\widetilde{\mathbf{H}}^H[k]\widetilde{\mathbf{H}}[k]\right|\right), \tag{4}$$

where γ represents the average subarray SNR after analog combining at the Rx, $U = \min(M, N)$.

2.2 Channel Model

Since mmWave channel is mainly determined by a LoS component and NLoS components, we use Ricean MIMO channel model here and the Ricean factor defined as the ratio of the LoS component power to the NLoS component power. For ease of analysis, we focus on the pure LoS MIMO channel hereinafter.

As illustrated in Fig. 1, we assume a pure LoS MIMO channel and let S_t and S_r denote the spacings between adjacent subarrays for the Tx and Rx, respectively, meeting the requirement $d \ll S_t, S_r \ll R$ where d and R denote the spacings of adjacent antenna elements and the distance between the Tx and Rx, respectively. We further assume that the received signals between different subarrays follow spherical wave model, while those within each subarray follow plane wave model, which are reflected in the distance between a pair of antenna elements at the Tx and Rx [24]. Therefore, the channel between the tth transmit antenna and the rth receive antenna, $h_{r,t}$ ($r = 0, 1, ..., MQ-1; t = 0, 1, ..., NP-1$), can be expressed as

$$h_{r,t} = e^{j2\pi f_c \frac{l_{r,t}}{c}}, \tag{5}$$

where f_c is the carrier frequency, c denotes the speed of light, and $l_{r,t}$ represents the distance between the corresponding antennas at the Tx and Rx given by

$$\begin{aligned} l_{r,t} =& l_{m,n}^{0,0} + pd\sin\theta_n^T - qd\sin\theta_m^R, \\ & r = mQ + q,\ t = nP + p, \end{aligned} \tag{6}$$

where θ_n^T ($n = 0, 1, ..., N-1$) and θ_m^R ($m = 0, 1, ..., M-1$) represent the angle of departure (AoD) of the nth transmit subarray and the angle of arrival (AoA) of the mth receive subarray, respectively. $p = 0, 1, ..., P-1$ and $q = 0, 1, ..., Q-1$ represent the antenna index of corresponding subarrays. $l_{m,n}^{0,0}$ is the distance between the reference elements of the nth transmit subarray and the mth receive subarray, and can be further calculated by [25]

$$\begin{aligned} l_{m,n}^{0,0} &= [(z_0 + mS_r\cos\theta - nS_t)^2 + (R + mS_r\sin\theta\cos\varphi)^2 \\ &\quad + (mS_r\sin\theta\sin\varphi)^2]^{\frac{1}{2}} \\ &\approx R + mS_r\sin\theta\cos\varphi \\ &\quad + \frac{(mS_r\sin\theta)^2 + (z_0 + mS_r\cos\theta - nS_t)^2}{2R}, \end{aligned} \tag{7}$$

where the Mclaughlin approximation formula of $(1+\triangle)^{\frac{1}{2}} \approx 1 + \frac{\triangle}{2}$ when $\triangle \ll 1$ is used for approximate calculation. As shown in Fig. 1, θ and φ are the angles of the Rx at coordinate system, and z_0 is the original position of the Rx along the z-axis. Considering a wideband mmWave LoS MIMO system, the frequency-domain channel response between the tth transmit antenna and the rth receive antenna, $h_{r,t}[k]$, is given by

$$h_{r,t}[k] = h_{r,t}e^{j2\pi f_k \frac{l_{r,t}}{c}} = e^{j2\pi(f_k + f_c)\frac{l_{r,t}}{c}}. \tag{8}$$

As a result, the channel matrix $\mathbf{H}[k]$ in Eq. (1) can be represented as

$$\mathbf{H}[k] = \begin{bmatrix} \mathbf{H}_{0,0}[k] & \cdots & \mathbf{H}_{0,N-1}[k] \\ \vdots & \ddots & \vdots \\ \mathbf{H}_{M-1,0}[k] & \cdots & \mathbf{H}_{M-1,N-1}[k] \end{bmatrix}, \tag{9}$$

where the subchannel matrix

$$\begin{aligned} \mathbf{H}_{m,n}[k] &= h_{m,n}^{0,0}[k]\begin{bmatrix} \widetilde{h}_{m,n}^{0,0}[k] & \cdots & \widetilde{h}_{m,n}^{0,P-1}[k] \\ \vdots & \ddots & \vdots \\ \widetilde{h}_{m,n}^{Q-1,0}[k] & \cdots & \widetilde{h}_{m,n}^{Q-1,P-1}[k] \end{bmatrix} \\ &= h_{m,n}^{0,0}[k]\mathbf{a}_R(k,\theta_m^R)\mathbf{a}_T^H(k,\theta_n^T), \end{aligned} \tag{10}$$

$h_{m,n}^{0,0}[k] = \exp\left(j2\pi(f_k + f_c)\frac{l_{m,n}^{0,0}}{c}\right)$, and $\widetilde{h}_{m,n}^{q,p}[k] = \exp\left(j2\pi(f_k + f_c)\frac{pd\sin\theta_n^T - qd\sin\theta_m^R}{c}\right)$, $\mathbf{a}_T(k,\theta_n^T)$ and $\mathbf{a}_R(k,\theta_m^R)$ represent the array response vectors of the nth transmit subarray and the mth receive subarray, respectively, given by

$$\begin{aligned} \mathbf{a}_T(k,\theta_n^T) =& \Big[1, \exp\left(j2\pi(f_k + f_c)\frac{d\sin\theta_n^T}{c}\right), ..., \\ & \exp\left(j2\pi(f_k + f_c)(P-1)\frac{d\sin\theta_n^T}{c}\right)\Big]^T \end{aligned} \tag{11}$$

and

$$\begin{aligned} \mathbf{a}_R(k,\theta_m^R) =& \Big[1, \exp\left(j2\pi(f_k + f_c)\frac{d\sin\theta_m^R}{c}\right), ..., \\ & \exp\left(j2\pi(f_k + f_c)(Q-1)\frac{d\sin\theta_m^R}{c}\right)\Big]^T. \end{aligned} \tag{12}$$

3. Impact of Subarray Separations on Spectral Efficiency

As stated in [13] and [16], the optimization of antenna/subarray placement is beneficial for the channel capacity in narrowband LoS MIMO systems with digital/hybrid arrays. When different columns or rows of the channel matrix satisfy orthogonality, the optimal antenna/subarray separation product (i.e., $S_t S_r = \frac{\lambda_c R}{D\cos\theta}$, assuming $D = \max(M, N)$) can be achieved, thus maximizing the spectral efficiency. However, due to the large bandwidth in wideband systems, different frequencies will lead to different subarray spacing designs. Therefore, we investigate this effect in the following.

At the frequency index k, the optimal subarray separation product can be expressed as $S_t[k]S_r[k] = \frac{\lambda_k R}{D\cos\theta}$, where $\lambda_k = \frac{c}{f_k + f_c}$. The RF equivalent channel matrix $\widetilde{\mathbf{H}}[k]$ is given by

$$\begin{aligned}\widetilde{\mathbf{H}}[k] &= \mathbf{W}^H\mathbf{H}[k]\mathbf{F} \\ &= \begin{bmatrix} \widetilde{H}_{0,0}[k] & \cdots & \widetilde{H}_{0,(N-1)}[k] \\ \vdots & \ddots & \vdots \\ \widetilde{H}_{(M-1),0}[k] & \cdots & \widetilde{H}_{(M-1),(N-1)}[k] \end{bmatrix},\end{aligned} \tag{13}$$

where $\widetilde{H}_{m,n}[k] = \mathbf{w}_m^H\mathbf{H}_{m,n}[k]\mathbf{f}_n$. In this paper, we use single beam in each subarray. Therefore, the normalized weight vectors $\mathbf{f}_n$ and $\mathbf{w}_m$ in Eq. (2) and Eq. (3) are given by

$$\begin{aligned}\mathbf{f}_n = &\frac{1}{\sqrt{P}}\Big[1, \exp\Big(-j2\pi f_c \frac{d\sin\widetilde{\theta}_n^T}{c}\Big), ..., \\ &\exp\Big(-j2\pi f_c (P-1)\frac{d\sin\widetilde{\theta}_n^T}{c}\Big)\Big]^T\end{aligned} \tag{14}$$

and

$$\begin{aligned}\mathbf{w}_m = &\frac{1}{\sqrt{Q}}\Big[1, \exp\Big(-j2\pi f_c \frac{d\sin\widetilde{\theta}_m^R}{c}\Big), ..., \\ &\exp\Big(-j2\pi f_c (Q-1)\frac{d\sin\widetilde{\theta}_m^R}{c}\Big)\Big]^T,\end{aligned} \tag{15}$$

respectively, which enable the main beam to point towards the direction represented by the angles $\widetilde{\theta}_n^T$ and $\widetilde{\theta}_m^R$. In order to investigate the sensitivity of the subarray separations designed at different frequencies, we set the frequency index related to a given subarray spacing design as k_1, $k_1 = 0, 1, ..., K-1$, and obtain

$$\begin{aligned}&\widetilde{\mathbf{H}}^H[k,k_1]\widetilde{\mathbf{H}}[k,k_1] \\ &= PQ\begin{bmatrix} G_{0,0}[k,k_1] & \cdots & G_{0,N-1}[k,k_1] \\ \vdots & \ddots & \vdots \\ G_{N-1,0}[k,k_1] & \cdots & G_{N-1,N-1}[k,k_1] \end{bmatrix},\end{aligned} \tag{16}$$

where $G_{n_1,n_2}[k,k_1] = \sum_{m=0}^{M-1}\exp\Big(j\frac{2\pi}{\lambda_k}\big(l_{m,n_2}^{0,0}[k_1] - l_{m,n_1}^{0,0}[k_1]\big)\Big)$, and $l_{m,n_2}^{0,0}[k_1] - l_{m,n_1}^{0,0}[k_1] = \frac{(2mn_1 - 2mn_2 + n_2^2 - n_1^2)\lambda_{k_1}}{2D\cos\theta}$, assuming $S_t[k_1] = S_r[k_1]$ and $z_0 = 0$. Furthermore, it is not difficult to obtain the spectral efficiency as a function of k_1 by substituting Eq. (16) into Eq. (4). Our aim is to find the optimal k_1 for the spectral efficiency optimization problem formulated as

$$k_1^* = \underset{k_1=0,1,...,K-1}{\arg\max}\left(\frac{1}{K}\sum_{k=0}^{K-1}\log_2\left(\left|\mathbf{I} + \frac{\gamma}{U}\widetilde{\mathbf{H}}^H[k,k_1]\widetilde{\mathbf{H}}[k,k_1]\right|\right)\right), \tag{17}$$

but it is difficult to solve due to the complicated log-determinant function. Nevertheless, we give the relationship between SE and f_{k_1} by exhaustive search as shown in Fig. 2 to find the optimal k_1, where different carrier frequencies and bandwidths are considered for comparison. It can be seen that the maximum spectral efficiency almost occurs at $f_{k_1} = 0$ (i.e., f_c) regardless of the variation of the carrier frequency and bandwidth, though the effect of k_1 on SE is negligible. Therefore, when the subarray spacing is limited, we can consider designing the subarray spacing according to the highest frequency point to reduce the array size. It

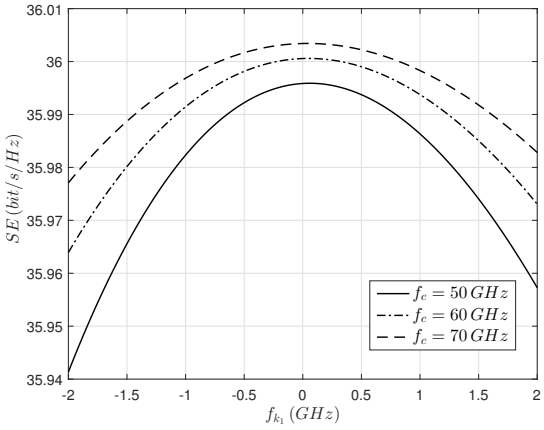

(a)

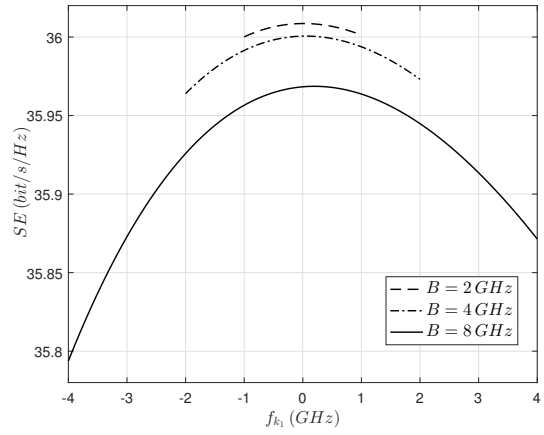

(b)

Fig. 2 SE versus f_{k_1}: (a) B = 4 GHz and f_c = 50 GHz, 60 GHz and 70 GHz; (b) f_c = 60 GHz and B = 2 GHz, 4 GHz and 8 GHz. R = 100 m, γ = 0 dB, $N = M = 4$, P = 128 and Q = 4.

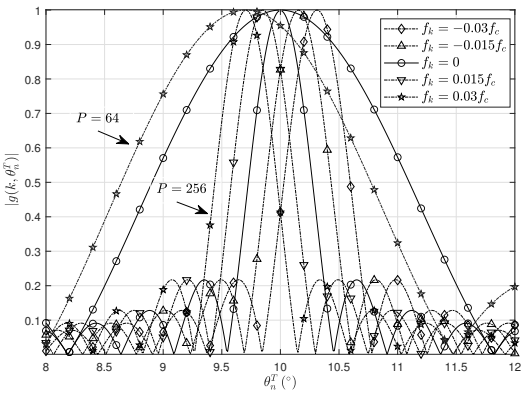

Fig. 3 Beam pattern versus different θ_n^T with $P = 64$ or 256, $\widetilde{\theta}_n^T = 10°$.

is also reasonable to design the Rayleigh distance criterion using the carrier frequency in wideband systems.

4. Beam Squint Analysis and Improved Analog Beamforming Design

4.1 Beam Squint Analysis

For a full-digital system, beam squint can be easily resolved through employing different steering vectors for beamforming at different frequencies. However, for a hybrid array system, beam squint is difficult to eliminate only through the adjustment of phase shifters, since phase shifter is essentially a narrowband device and thus generally designed for a specific frequency, e.g., the carrier frequency [21]. In wideband case, the beam pattern $g(k,\theta_n^T)$ of the nth transmit subarray not only depends on the angle of beam but also the frequency, which is significantly different from the narrowband case. From Eq. (11) and Eq. (14), we have

$$\begin{aligned} & g(k,\theta_n^T) \\ &= (\mathbf{a}_T(k,\theta_n^T))^T\mathbf{f}_n \\ &= \frac{1}{\sqrt{P}}\exp\left(j\pi(P-1)\frac{d}{c}\left[(f_k+f_c)\sin\theta_n^T - f_c\sin\widetilde{\theta}_n^T\right]\right) \\ &\quad\cdot\frac{\sin\left(P\pi\frac{d}{c}\left[(f_k+f_c)\sin\theta_n^T - f_c\sin\widetilde{\theta}_n^T\right]\right)}{\sin\left(\pi\frac{d}{c}\left[(f_k+f_c)\sin\theta_n^T - f_c\sin\widetilde{\theta}_n^T\right]\right)}, \end{aligned} \tag{18}$$

whose peak appears at the beam direction of $\theta_{max} = \arcsin\left(\frac{\sin\widetilde{\theta}_n^T}{1+f_k/f_c}\right)$. Only when $f_k = 0$, θ_{max} can point to the expected angle $\widetilde{\theta}_n^T$, and there will be angle deviation in other case. It implies that the expected beam direction associated with the phase shifters varies with the frequency, leading to the beam squint. Fig. 3 illustrates a beam squint example for different frequencies. It can be seen from the figure that, in the expected beam direction, the largest peak occurs only at $f_k = 0$ (i.e., the carrier frequency), and the beamforming gain incurs increasing loss with f_k deviating from f_c. It means that beam squint with larger bandwidth can cause further loss. As the number of antenna elements increases, the beamwidth becomes narrower and the beamforming gain falls more rapidly in the expected beam direction.

Assuming that AoD and AoA are perfectly available, i.e., $\widetilde{\theta}_n^T = \theta_n^T$ and $\widetilde{\theta}_m^R = \theta_m^R$, the RF equivalent subchannel between the nth transmit subarray and the mth receive subarray can be expressed as

$$\begin{aligned} & \widetilde{H}_{m,n}[k] \\ &= \mathbf{w}_m^H\mathbf{H}_{m,n}[k]\mathbf{f}_n \\ &= \frac{1}{\sqrt{PQ}}\exp\left(j2\pi(f_k+f_c)\frac{R}{c}\right) \\ &\quad\cdot\sum_{p=0}^{P-1}\sum_{q=0}^{Q-1}\exp\left(j2\pi f_k\frac{pd\sin\theta_n^T - qd\sin\theta_m^R}{c}\right) \\ &= \frac{1}{\sqrt{PQ}}\frac{\sin\left(P\pi f_k\frac{d\sin\theta_n^T}{c}\right)\sin\left(Q\pi f_k\frac{d\sin\theta_m^R}{c}\right)}{\sin\left(\pi f_k\frac{d\sin\theta_n^T}{c}\right)\sin\left(\pi f_k\frac{d\sin\theta_m^R}{c}\right)} \\ &\quad\cdot\exp\left(j\pi\frac{f_k d}{c}\left[2\left(1+\frac{f_c}{f_k}\right)\frac{R}{d} + (P-1)\sin\theta_n^T - (Q-1)\sin\theta_m^R\right]\right). \end{aligned} \tag{19}$$

As $\sin\left(P\pi f_k\frac{d\sin\theta_n^T}{c}\right)\sin\left(Q\pi f_k\frac{d\sin\theta_m^R}{c}\right)$ and $\sin\left(\pi f_k\frac{d\sin\theta_n^T}{c}\right)\sin\left(\pi f_k\frac{d\sin\theta_m^R}{c}\right)$ have different periods, zero crossing inevitably occurs when the number of antennas and bandwidth are relatively large, and it exhibits frequency-selective deep fading in the RF equivalent channel, which will be illustrated in Fig. 4.

4.2 Improved Analog Beamforming for Phase Compensation

Due to the beamforming gain loss caused by beam squint, we need to design appropriate phase shifter values with flat characteristics in the frequency-domain to eliminate frequency-selective deep fading. Note that ZC sequence is a well-known constant amplitude zero autocorrelation (CAZAC) sequence and its Fourier transform is also constant-envelope, which enables omnidirectional radiation pattern in massive MIMO systems [26]. Therefore, we adopt it to compensate the conventional analog beamforming vector.

Define the compensation vectors as $\mathbf{f}_{c,n} = [\exp(-j\phi_{c,n}^0), \exp(-j\phi_{c,n}^1), ..., \exp(-j\phi_{c,n}^{P-1})]^T$ and $\mathbf{w}_{c,m} = [\exp(-j\psi_{c,m}^0), \exp(-j\psi_{c,m}^1), ..., \exp(-j\psi_{c,m}^{Q-1})]^T$, then the analog precoding vector and combining vector after phase compensation become

$$\begin{aligned} \widetilde{\mathbf{f}}_n &= \mathbf{f}_n \odot \mathbf{f}_{c,n} \\ &= \frac{1}{\sqrt{P}}\big[\exp(-j(\phi_n^0 + \phi_{c,n}^0)), \exp(-j(\phi_n^1 + \phi_{c,n}^1)), \\ &\quad ..., \exp(-j(\phi_n^{P-1} + \phi_{c,n}^{P-1}))\big]^T \end{aligned} \tag{20}$$

and

$$\begin{aligned}\widetilde{\mathbf{w}}_m &= \mathbf{w}_m \odot \mathbf{w}_{c,m} \\ &= \frac{1}{\sqrt{Q}}\big[\exp(-j(\psi_m^0+\psi_{c,m}^0)), \exp(-j(\psi_m^1+\psi_{c,m}^1)), \\ &\quad ..., \exp(-j(\psi_m^{Q-1}+\psi_{c,m}^{Q-1}))\big]^T,\end{aligned} \tag{21}$$

where $\phi_n^p = 2\pi p f_c d \sin\widetilde{\theta}_n^T/c$ and $\psi_m^q = 2\pi q f_c d \sin\widetilde{\theta}_m^R/c$. Replacing $\mathbf{f}_n$ and $\mathbf{w}_m$ in Eq. (19) with $\widetilde{\mathbf{f}}_n$ and $\widetilde{\mathbf{w}}_m$, the RF equivalent channel becomes

$$\begin{aligned}\widetilde{H}_{m,n}[k] =& \frac{1}{\sqrt{PQ}} \exp\left(j2\pi(f_k+f_c)\frac{R}{c}\right) \\ &\cdot \sum_{p=0}^{P-1}\sum_{q=0}^{Q-1}\left\{\exp\left(j\left(2\pi f_k \frac{pd\sin\theta_n^T}{c} - \phi_{c,n}^p\right)\right)\right. \\ &\left.\cdot \exp\left(j\left(\psi_{c,m}^q - 2\pi f_k \frac{qd\sin\theta_m^R}{c}\right)\right)\right\}.\end{aligned} \tag{22}$$

Since the compensation vectors $\mathbf{f}_{c,n}$ and $\mathbf{w}_{c,m}$ have the similar form, we only consider the design for $\mathbf{f}_{c,n}$ based on the ZC sequence [27], and it is given by

$$\exp(j\phi_{c,n}^p) = \begin{cases}\exp(j\pi\frac{rp(p+2q')}{P}), & P \text{ is even} \\ \exp(j\pi\frac{rp(p+2q'+1)}{P}), & P \text{ is odd}\end{cases} \tag{23}$$

where q' and r are parameters and will be calculated in the following.

Our aim is to use $\exp\left(j\phi_{c,n}^p\right)$ to avoid the occurrence of frequency-selective deep fading in $\widetilde{H}_{m,n}[k]$ by exploiting the characteristic of ZC sequence. As the phase shifters for conventional beamforming can only be set for a specific frequency, we design $\phi_{c,n}^p$ to compensate phases evenly within $\left[-\frac{B}{2}, \frac{B}{2}\right]$ instead of a specific frequency, which sacrifices part of array gain to allow the power evenly distributed across the whole operating frequency band. We define $u = \frac{f_k d\sin\theta_n^T}{c}$ in Eq. (22) and $u \in \left[-\frac{Bd\sin\theta_n^T}{2c}, \frac{Bd\sin\theta_n^T}{2c}\right]$. In Eq. (23), when P is even, we take the derivative of the variable p in the phase of $\exp\left(j\phi_{c,n}^p\right)$, and obtain $\left[\frac{rp(p+2q')}{2P}\right]' = \frac{r(p+q')}{P}$, which increases monotonically with p. Particularly when $p = 0$ and $p = P-1$, we have the minimum and maximum values of the corresponding derivative, i.e., $\frac{rq'}{P}$ and $\frac{r(P-1+q')}{P}$, respectively, and thus the compensation frequency range is $\left[\frac{rq'}{P}, \frac{r(P-1+q')}{P}\right]$. To guarantee the compensation frequency and u to be located in the same range, we have

$$\begin{cases}\frac{rq'}{P} = -\frac{Bd\sin\theta_n^T}{2c} \\ \frac{r(P-1+q')}{P} = \frac{Bd\sin\theta_n^T}{2c}\end{cases}. \tag{24}$$

Solving Eq. (24), we have $r = \frac{PBd\sin\theta_n^T}{c(P-1)}$ and $q' = -\frac{P-1}{2}$. Similarly, when P is odd, we have $r = \frac{PBd\sin\theta_n^T}{c(P-1)}$ and $q' = -\frac{P}{2}$. Substituting r and q' in the above two cases respectively into Eq. (23), we can obtain the same compensatory phases given by

$$\phi_{c,n}^p = -\frac{\pi B}{c}pd\sin\theta_n^T + \frac{\pi Bdp^2\sin\theta_n^T}{c(P-1)}. \tag{25}$$

Likewise, the compensatory phase at the Rx can be also obtained,

$$\psi_{c,m}^q = -\frac{\pi B}{c}qd\sin\theta_m^R + \frac{\pi Bdq^2\sin\theta_m^R}{c(Q-1)}. \tag{26}$$

5. SNR Maximization with Improved Analog Beamforming

Because the orthogonal frequency division multiplexing (OFDM) signal has excessively high peak to average power ratio, SC-FDE scheme is more attractive for high-throughput wideband mmWave communication systems [28]. It is necessary to equalize the received symbols to remove the ISI caused by frequency-selective RF equivalent channel. In this section, we consider the linear SC-FDE for ISI mitigation in wideband mmWave LoS MIMO systems, and evaluate the equalization performance on the SNR after equalization.

In SC-FDE systems, a cyclic prefix (CP) is generally inserted in front of the block data to convert the linear convolution of the transmitted signal and the wireless channel into a circular convolution, which can prevent the inter-block interference (IBI). We assume that the length of CP is larger than the delay spread of the channel. At the Rx, we remove the CP, and then perform $K = \rho L$ points fast Fourier transform (FFT) and frequency-domain equalization, where ρ is the up-sampling ratio and L is the length of symbol block. Finally, we perform IFFT to convert the frequency-domain signal to the time-domain for detection. Let the frequency-domain received signal vector after analog combining expressed as $\overline{\mathbf{y}} = [\mathbf{y}_0^T, \mathbf{y}_1^T, ..., \mathbf{y}_{M-1}^T]^T$, where $\mathbf{y}_m = [y_m[0], y_m[1] ... , y_m[K-1]]^T$ denote the frequency-domain sampled symbol vector of the mth subarray, and it is given by

$$\overline{\mathbf{y}} = \overline{\mathbf{H}}\overline{\mathbf{x}} + \overline{\mathbf{n}}, \tag{27}$$

where $\overline{\mathbf{x}} = [\mathbf{x}_0^T, \mathbf{x}_1^T, ..., \mathbf{x}_{N-1}^T]^T$ and $\overline{\mathbf{n}} = [\overline{\mathbf{n}}_0^T, \overline{\mathbf{n}}_1^T, ..., \overline{\mathbf{n}}_{M-1}^T]^T$ denote the frequency-domain transmitted signal vector and noise vector, respectively. And

$$\overline{\mathbf{H}} = \begin{bmatrix}\overline{\mathbf{H}}_{0,0} & \cdots & \overline{\mathbf{H}}_{0,N-1} \\ \vdots & \ddots & \vdots \\ \overline{\mathbf{H}}_{M-1,0} & \cdots & \overline{\mathbf{H}}_{M-1,N-1}\end{bmatrix}, \tag{28}$$

where $\overline{\mathbf{H}}_{m,n} = diag(\widetilde{H}_{m,n}[0], ..., \widetilde{H}_{m,n}[K-1])$.

Let $\mathbf{G}_{ZF} \in \mathbb{C}^{NK\times MK}$ denote the frequency-domain ZF equalization matrix, and it is given by

$$\mathbf{G}_{ZF} = (\overline{\mathbf{H}}^H\overline{\mathbf{H}})^{-1}\overline{\mathbf{H}}^H. \tag{29}$$

Therefore, the received signal vector after ZF equalization can be expressed as

$$\begin{aligned}\widetilde{\mathbf{y}}_{ZF} &= \mathbf{G}_{ZF}\overline{\mathbf{y}} \\ &= \overline{\mathbf{x}} + \left(\overline{\mathbf{H}}^H\overline{\mathbf{H}}\right)^{-1}\overline{\mathbf{H}}^H\overline{\mathbf{n}} \\ &= \overline{\mathbf{x}} + \widetilde{\mathbf{n}}_{ZF}.\end{aligned} \tag{30}$$

The noise power can be represented as

$$\begin{aligned}&E\{\|\widetilde{\mathbf{n}}_{ZF}\|^2\} \\ &= E\left\{\left\|\left(\overline{\mathbf{H}}^H\overline{\mathbf{H}}\right)^{-1}\overline{\mathbf{H}}^H\overline{n}\right\|^2\right\} \\ &= tr\left\{E\left\{\left(\left(\overline{\mathbf{H}}^H\overline{\mathbf{H}}\right)^{-1}\overline{\mathbf{H}}^H\overline{n}\right)\left(\left(\overline{\mathbf{H}}^H\overline{\mathbf{H}}\right)^{-1}\overline{\mathbf{H}}^H\overline{n}\right)^H\right\}\right\} \\ &= \sigma^2 tr\left\{\left(\overline{\mathbf{H}}^H\overline{\mathbf{H}}\right)^{-1}\right\}.\end{aligned} \tag{31}$$

The SNR after ZF equalization is given by

$$\overline{\gamma}_{ZF} = \frac{\chi^2}{E\{\|\widetilde{\mathbf{n}}_{ZF}\|^2\}/NK} = \overline{\gamma}\frac{NK}{tr\left\{\left(\overline{\mathbf{H}}^H\overline{\mathbf{H}}\right)^{-1}\right\}}. \tag{32}$$

where $\overline{\gamma} = \frac{\chi^2}{\sigma^2} = \gamma + 10\log_{10}(P \times Q)$ represents the element SNR and χ^2 denotes the average signal power.

With MMSE equalization, the corresponding equalization matrix can be given by

$$\mathbf{G}_{MMSE} = \left(\overline{\mathbf{H}}^H\overline{\mathbf{H}} + \frac{1}{\overline{\gamma}}\mathbf{I}_{NK}\right)^{-1}\overline{\mathbf{H}}^H, \tag{33}$$

and its corresponding MMSE is derived by

$$\begin{aligned}&E\{\|\mathbf{G}_{MMSE}\overline{\mathbf{y}} - \overline{\mathbf{x}}\|^2\} \\ &= tr\left\{E\left\{\left(\mathbf{G}_{MMSE}\overline{\mathbf{y}} - \overline{\mathbf{x}}\right)\overline{\mathbf{y}}^H\mathbf{G}_{MMSE}^H\right\}\right\} \\ &\quad + tr\left\{E\left\{\left(\overline{\mathbf{x}} - \mathbf{G}_{MMSE}\overline{\mathbf{y}}\right)\overline{\mathbf{x}}^H\right\}\right\} \\ &\overset{(a)}{=} tr\left\{E\left\{\left(\overline{\mathbf{x}} - \mathbf{G}_{MMSE}\overline{\mathbf{y}}\right)\overline{\mathbf{x}}^H\right\}\right\} \\ &= \chi^2 tr\left\{\mathbf{I}_{NK} - \left(\overline{\mathbf{H}}^H\overline{\mathbf{H}} + \frac{1}{\overline{\gamma}}\mathbf{I}_{NK}\right)^{-1}\overline{\mathbf{H}}^H\overline{\mathbf{H}}\right\},\end{aligned} \tag{34}$$

where (a) holds in terms of the orthogonality principle, i.e., $E\left\{\left(\mathbf{G}_{MMSE}\overline{\mathbf{y}} - \overline{\mathbf{x}}\right)\overline{\mathbf{y}}^H\right\} = 0$. Therefore, the SNR after MMSE equalization is

$$\begin{aligned}\overline{\gamma}_{MMSE} &= \frac{\chi^2 - E\{\|\mathbf{G}_{MMSE}\overline{\mathbf{y}} - \overline{\mathbf{x}}\|^2\}/NK}{E\{\|\mathbf{G}_{MMSE}\overline{\mathbf{y}} - \overline{\mathbf{x}}\|^2\}/NK} \\ &= \frac{tr\left\{\left(\overline{\mathbf{H}}^H\overline{\mathbf{H}} + \frac{1}{\overline{\gamma}}\mathbf{I}_{NK}\right)^{-1}\overline{\mathbf{H}}^H\overline{\mathbf{H}}\right\}}{NK - tr\left\{\left(\overline{\mathbf{H}}^H\overline{\mathbf{H}} + \frac{1}{\overline{\gamma}}\mathbf{I}_{NK}\right)^{-1}\overline{\mathbf{H}}^H\overline{\mathbf{H}}\right\}}.\end{aligned} \tag{35}$$

6. Simulation Results

In this section, we present the simulation results to demonstrate the performance of the improved analog beamforming in SC-FDE based mmWave LoS MIMO systems. We assume that the Tx and Rx are placed in parallel, i.e., $\theta = 0°$. This means that AoD and AoA have the same value, i.e., $\theta_n^T = \theta_m^R$. Unless stated otherwise, we consider $N_s = M = N = 4$, $P = 128$, $Q = 4$, the carrier frequency of 60 GHz and the bandwidth of 4 GHz. We choose $S_t = S_r = \sqrt{\frac{\lambda_c R}{M\cos\theta}}$ and $d = \frac{c}{2f_c}$ as the subarray separation for a practical array placement to meet the Rayleigh distance criterion at $R = 100$ m. The reference baseband signal is a quadrature phase shift keying (QPSK) modulated signal filtered by a raised cosine filter with roll-off factor $\epsilon = 0.2$. The length of symbol block $L = 512$ and CP length $L_{cp} = 64$. Up-sampling ratio $\rho = 2$ and FFT size at the Rx $K = \rho L = 1024$.

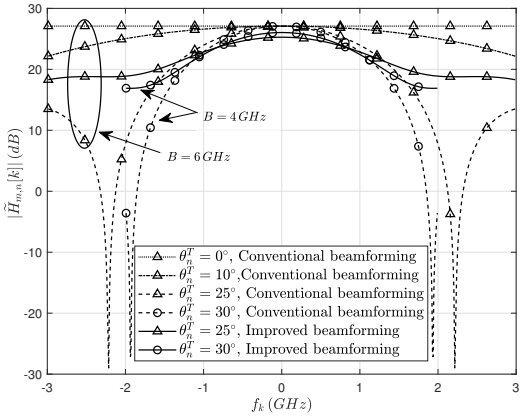

Fig. 4 The comparison of the RF equivalent channel frequency-domain response with beam squint.

Fig. 4 compares the frequency-domain response of the RF equivalent channel with different AoDs. It can be seen that due to the influence of beam squint on conventional beamforming, larger AoD leads to more severe frequency-selective fading. As θ_n^T increases, deep fading appears in the frequency-domain response of the RF equivalent channel, which will seriously affect signal transmission. Although the improved beamforming causes slight beamforming gain loss around the carrier frequency, it can effectively eliminate the frequency-selective deep fading caused by beam squint with tens dB gain when $B = 4$ GHz or 6 GHz, greatly improving the reliability of a wideband system.

Fig. 5 shows the BER performance versus $\overline{\gamma}$ when $\theta_n^T = 25°$. Note that the element SNR of $\overline{\gamma} = -20$ dB corresponds to the subarray SNR $\gamma = 7$ dB because the Tx/Rx subarrays have 128 and 4 elements, respectively (the beamforming gain is $10\log_{10}(128 \times 4) = 27$ dB). It can be seen that the improved beamforming has an approximately 3 dB performance improvement over the conventional beamforming using ZF equalization, since the deep fading points of equivalent channel are effectively removed. Here, we take the performance with the TTD lines as the optimal one for comparison, which outperforms the improved one over 5 dB due to beamforming loss caused by beam squint. The MMSE equalization has slightly better performance than the ZF equalization.

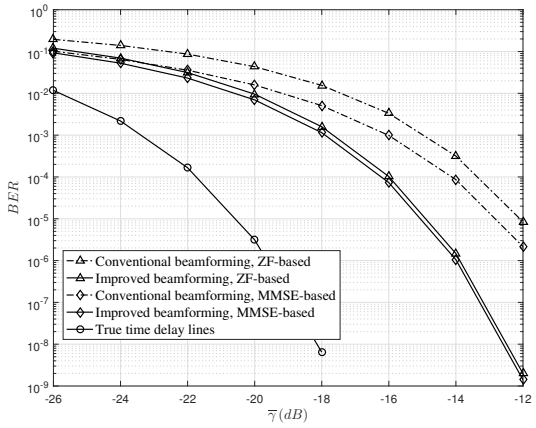

Fig. 5 BER performance versus $\overline{\gamma}$ with $\theta_n^T = 25°$, $B = 4$ GHz.

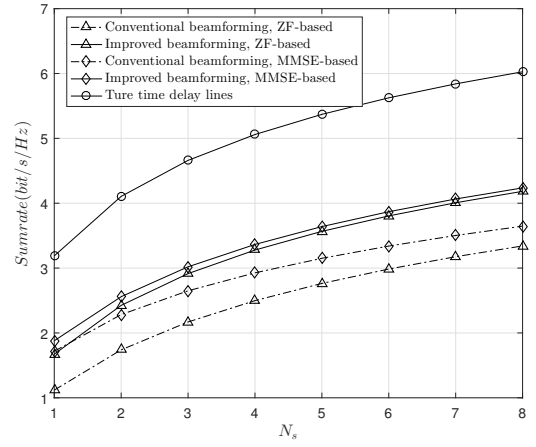

Fig. 6 Sum rate versus the number of data stream under $\overline{\gamma} = -18$ dB.

Fig. 6 shows the sum rate after equalization versus the number of data stream N_s from 1 to 8, where we assume that the number of both subarrays and RF chains are always equal to N_s, i.e., $M = N = N_s$. It is observed that the sum rate is improved with the increasing number of data steams, and using the improved beamforming achieves higher sum rate than conventional beamforming. The gap between them gets large as N_s increases, and achieves 0.8 bits/s/Hz when ZF equalization is used for eight data streams. The sum rate using the improved beamforming with ZF equalization approaches that with MMSE equalization as the number of data steam increases.

7. Conclusions

In this paper, we have investigated the influence of frequency-dependency on the optimal subarray separations for wideband mmWave LoS MIMO systems using hybrid arrays, and shown that the Rayleigh distance designed under carrier frequency can achieve the maximum spectral efficiency. Through the analysis of beam squint effect on the RF equivalent channel, an improved analog beamforming can be achieved by adjusting phase shifter values with ZC sequence to, compensate the frequency-selective deep fading. With the improved analog beamforming, the equalization performance in term of output SNR using ZF and MMSE based equalizers in a SC-FDE system is investigated. Numerical results demonstrate the effectiveness of the improved analog beamforming in terms of overcoming the beam squint effect.

References

[1] A. L. Swindlehurst, E. Ayanoglu, P. Heydari and F. Capolino, "Millimeter-wave massive MIMO: the next wireless revolution?," IEEE Commun. Mag., vol. 52, no. 9, pp. 56-62, Sept. 2014.

[2] R. W. Heath, N. González-Prelcic, S. Rangan, W. Roh and A. M. Sayeed, "An overview of signal processing techniques for millimeter wave MIMO systems," IEEE J. Sel. Top. Signal Process., vol. 10, no. 3, pp. 436-453, Apr. 2016.

[3] J. G. Andrews et al., "What will 5G be?," IEEE J. Sel. Areas Commun., vol. 32, no. 6, pp. 1065-1082, Jun. 2014.

[4] Z. Pi and F. Khan, "An introduction to millimeter-wave mobile broadband systems," IEEE Commun. Mag., vol. 49, no. 6, pp. 101-107, Jun. 2011.

[5] J. Hoydis, S. ten Brink and M. Debbah, "Massive MIMO in the UL/DL of cellular networks: how many antennas do we need?," IEEE J. Sel. Areas Commun., vol. 31, no. 2, pp. 160-171, Feb. 2013.

[6] T. S. Rappaport et al., "Millimeter wave mobile communications for 5G cellular: it will work!," in IEEE Access, vol. 1, pp. 335-349, 2013.

[7] A. F. Molisch, M. Steinbauer, M. Toeltsch, E. Bonek and R. S. Thoma, "Capacity of MIMO systems based on measured wireless channels," IEEE J. Sel. Areas Commun., vol. 20, no. 3, pp. 561-569, Apr. 2002.

[8] X. Yu, J. -C. Shen, J. Zhang and K. B. Letaief, "Alternating minimization algorithms for hybrid precoding in millimeter wave MIMO systems," IEEE J. Sel. Top. Signal Process., vol. 10, no. 3, pp. 485-500, Apr. 2016.

[9] J. A. Zhang, X. Huang, V. Dyadyuk and Y. J. Guo, "Massive hybrid antenna array for millimeter-wave cellular communications," IEEE Wirel. Commun., vol. 22, no. 1, pp. 79-87, Feb. 2015.

[10] F. Sohrabi and W. Yu, "Hybrid digital and analog beamforming design for large-scale antenna arrays," IEEE J. Sel. Top. Signal Process., vol. 10, no. 3, pp. 501-513, Apr. 2016.

[11] X. Huang and Y. J. Guo, "Frequency-domain AoA estimation and beamforming with wideband hybrid arrays," IEEE Trans. Wirel. Commun., vol. 10, no. 8, pp. 2543-2553, Aug. 2011.

[12] L. Zhou and Y. Ohashi, "Low complexity millimeter-wave LOS-MIMO precoding systems for uniform circular arrays," 2014 IEEE Wireless Communications and Networking Conference (WCNC), Istanbul, Turkey, 2014, pp. 1293-1297.

[13] F. Bohagen, P. Orten and G. E. Oien, "Design of optimal high-rank line-of-sight MIMO channels," IEEE Trans. Wirel. Commun., vol. 6, no. 4, pp. 1420-1425, Apr. 2007.

[14] L. Zhu and J. Zhu, "Optimal design of uniform circular antenna array in mmWave LOS MIMO channel," in IEEE Access, vol. 6, pp. 61022-61029, 2018.

[15] F. Bohagen, P. Orten and G. E. Oien, "Optimal design of uniform planar antenna arrays for strong line-of-sight MIMO channels," 2006 IEEE 7th Workshop on Signal Processing Advances in Wireless Communications, Cannes, France, 2006, pp. 1-5.

[16] Deng, J.; Li, H.; Zhang, J.A.; Huang, X.; Cheng, Z. "Transceiver optimization for mmWave line-of-sight MIMO systems using hybrid arrays," Micromachines 2023, 14, 236.

[17] B. Wang, F. Gao, S. Jin, H. Lin and G. Y. Li, "Spatial- and frequency-wideband effects in millimeter-wave massive MIMO systems," IEEE Trans. Signal Process., vol. 66, no. 13, pp. 3393-3406, Jul. 2018.

[18] R. Rotman, M. Tur and L. Yaron, "True time delay in phased arrays," in Proceedings of the IEEE, vol. 104, no. 3, pp. 504-518, Mar. 2016.

[19] M. Cai et al., "Effect of wideband beam squint on codebook design in phased-array wireless systems," 2016 IEEE Global Communications Conference (GLOBECOM), 2016, pp. 1-6.
[20] Zhiqiang WANG, Jiawei LIU, Jun WANG, Guangrong YUE, "Beam squint effect on high-throughput millimeter-wave communication with an ultra-massive phased array," Front. Inform. Technol. Electron. Eng., 2021, 22(4): 560–570.
[21] F. Gao, B. Wang, C. Xing, J. An and G. Y. Li, "Wideband beamforming for hybrid massive MIMO terahertz communications," IEEE J. Sel. Areas Commun., vol. 39, no. 6, pp. 1725-1740, Jun. 2021.
[22] N. J. Myers and R. W. Heath, "Infocus: a spatial coding technique to mitigate misfocus in near-field LoS beamforming," IEEE Trans. Wirel. Commun., vol. 21, no. 4, pp. 2193-2209, Apr. 2022.
[23] J. Huang, C. -X. Wang, R. Feng, J. Sun, W. Zhang and Y. Yang, "Multi-frequency mmWave massive MIMO channel measurements and characterization for 5G wireless communication systems," IEEE J. Sel. Areas Commun., vol. 35, no. 7, pp. 1591-1605, Jul. 2017.
[24] F. Bohagen, P. Orten and G. E. Oien, "On spherical vs. plane wave modeling of line-of-sight MIMO channels," IEEE Trans. Commun., vol. 57, no. 3, pp. 841-849, Mar. 2009.
[25] C. Xue, S. He, F. Ou, M. Wei, Y. Huang and L. Yang, "Asymmetric subarray structure design for mmWave LoS MIMO communication systems," 2016 IEEE/CIC International Conference on Communications in China (ICCC), 2016, pp. 1-6.
[26] X. Meng, X. -G. Xia and X. Gao, "Constant-envelope omni-directional transmission with diversity in massive MIMO systems," 2014 IEEE Global Communications Conference, Austin, TX, USA, 2014, pp. 3784-3789
[27] D. Chu, "Polyphase codes with good periodic correlation properties (Corresp.)," IEEE Trans. Inf. Theory, vol. 18, no. 4, pp. 531-532, Jul. 1972.
[28] S. Buzzi, C. D'Andrea, T. Foggi, A. Ugolini and G. Colavolpe, "Single-carrier modulation versus OFDM for millimeter-wave wireless MIMO," IEEE Trans. Commun., vol. 66, no. 3, pp. 1335-1348, Mar. 2018.

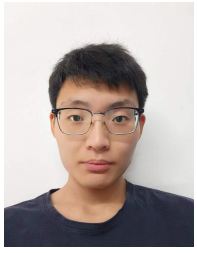

Yongpeng Hu received the B.E. degree from Zhengzhou University of Light Industry in 2021. He is currently working toward the M.E. degree at the School of Electronics and Information, Hangzhou Dianzi University, Hangzhou, China. His current research interests include millimeter wave communications and MIMO systems.

Hang Li received the B.Eng. and M.Eng. degrees in electronic engineering from Beijing Jiaotong University, Beijing, China, in 2003 and 2006, respectively, and the Ph.D. degree in electronic engineering from the University of Western Australia, Perth, WA, Australia, in 2014. From 2016 to 2019, he was a Post-Doctoral Research Fellow with the Global Big Data Technologies Centre, University of Technology Sydney, Sydney, NSW, Australia. He is currently a Professor with the School of Electronics and Information Engineering, Hangzhou Dianzi University, Hangzhou, China. His research interests include wireless communications signal processing and mm-wave massive MIMO.

J. Andrew Zhang received B.Sc. degree from Xi'an JiaoTong University, China, in 1996, M.Sc. degree from Nanjing University of Posts and Telecommunications, China, in 1999, and Ph.D. degree from the Australian National University, in 2004. Currently, He is a Professor in the School of Electrical and Data Engineering, University of Technology Sydney, Australia. Dr. Zhang's research interests are in the area of signal processing for wireless communications and sensing. He has published 250 papers in leading international Journals and conference proceedings, and has won 5 best paper awards for his work.

Xiaojing Huang received the B.Eng., M.Eng., and Ph.D. degrees in electronic engineering from Shanghai Jiao Tong University, Shanghai, China, in 1983, 1986, and 1989, respectively. He was a Principal Research Engineer with the Motorola Australian Research Center, Botany, NSW, Australia, from 1998 to 2003, and an Associate Professor with the University of Wollongong, Wollongong, NSW, Australia, from 2004 to 2008. He had been a Principal Research Scientist with the Commonwealth Scientific and Industrial Research Organisation (CSIRO), Sydney, NSW, Australia, and the Project Leader of the CSIRO Microwave and mm-Wave Backhaul projects since 2009. He is currently a Professor of Information and Communications Technology with the School of Electrical and Data Engineering and the Program Leader for Mobile Sensing and Communications with the Global Big Data Technologies Center, University of Technology Sydney (UTS), Sydney, NSW, Australia. His research interests include high-speed wireless communications, digital and analog signal processing, and synthetic aperture radar imaging. With over 33 years of combined industrial, academic, and scientific research experience, he has authored over 400 book chapters, refereed journal and conference papers, major commercial research reports, and filed 31 patents. Prof. Huang was a recipient of the CSIRO Chairman's Medal and the Australian Engineering Innovation Award in 2012 for exceptional research achievements in multigigabit wireless communications.

Zhiqun Cheng received the B.S. and M.S. degrees in microelectronics from Hefei University of Technology, Hefei, China, in 1986 and 1995, respectively, and the Ph.D. degree in icroelectronics and solid-state electronics from the Shanghai Institute of Microsystem and Information Technology, Chinese Academy of Sciences, Shanghai, China, in 2000.He is currently a Professor with the Department of Information Engineering,Hangzhou Dianzi University, Hangzhou, China, and a Senior Visiting Scholar with the Department of Electronic and Computer Engineering, Hong Kong University of Science and Technology (HKUST), Hong Kong. Prior to joining HKUST, he was a Lecturer with the Hefei University of Technology, Hefei, China (1986–1997) and an Associate Professor with the Shanghai Institute of Microsystem and Information Technology, Chinese Academy of Sciences, Shanghai, China (2000–2005). He has carried out research on GaAs HBTs and GaN HEMTs and has been involved with the design of compound semiconductor digital integrated circuits and RF transceivers. He has authored or coauthored 50 technical papers in journals and conference proceedings. His interests focus on III–V high-power and low-noise devices and circuits for microwave and millimeter applications and high-speed Si and SiGe devices and T/R systems and wireless communications.